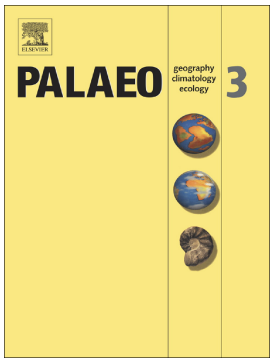

Reconstruction of palaeoclimate in Shalaii Cave, SE of Sangaw, Kurdistan Province of Iraq

Diary Ali Mohammed Amin, Sozan Burhan Ismaeel, Mark Altaweel

PII: S0031-0182(19)30068-9
DOI: https://doi.org/10.1016/j.palaeo.2019.03.044
Reference: PALAEO 9143

To appear in: *Palaeogeography, Palaeoclimatology, Palaeoecology*

Received date: 20 January 2019
Revised date: 28 March 2019
Accepted date: 28 March 2019

Please cite this article as: D.A.M. Amin, S.B. Ismaeel and M. Altaweel, Reconstruction of palaeoclimate in Shalaii Cave, SE of Sangaw, Kurdistan Province of Iraq, Palaeogeography, Palaeoclimatology, Palaeoecology, https://doi.org/10.1016/j.palaeo.2019.03.044

Reconstruction of paleoclimate in Shalaii Cave, SE of Sangaw, Kurdistan Province of Iraq

Diary Ali Mohammed amin[1], Sozan Burhan Ismaeel[1], Mark Altaweel[2]

[1]Department of Geology, College of Science, University of Sulaimani, Iraq
E-mail: diary.amin@univsul.edu.iq

[1] Department of Geology, College of Science, University of Sulaimani, Iraq
Email: adiary22@gmail.com

[2] Institute of Archaeology, University College London
Email: m.altaweel@ucl.ac.uk

Abstract

Shalaii Cave is a closed system cave that contains old and active speleothems. It is located on the northeast limb of the Ashdagh anticline in Sangaw district in northeastern Iraq. The study presents new data on cave monitoring and the geochemistry of stalagmite archives relevant for the paleoclimate of Iraq. An extensive cave monitoring program was conducted from June 2014 to March 2015, which included analyses of cave air temperature, relative humidity, cave air, dripwater, and modern calcite precipitates on glass slides. Physical parameters were measured monthly and continuously using data loggers and meteorological data; rainwater and dripwater samples were acquired for stable isotope analyses and hydrochemistry analysis. Stable isotopes of oxygen and carbon and absolute dating of U/Th series dating was used to determine palaeoclimate conditions. The microclimate of Shalaii Cave during the studied period (June-2014 to March-2015), the average temperature at the entrance point and inside the monitored cave was 17.05 °C and 20.18 °C respectively. The relative humidity at the entrance point and inside the cave was 66.6 % and 100 % respectively. Eleven samples of dripwater and five samples of rainwater were acquired for isotope analyses and thirteen samples of dripwater for hydrochemical analysis. From the environmental isotopes analysis (^{2}H and ^{18}O), all water samples fall between the global meteoric water line (GMWL) and Sangaw meteoric water line (SMWL). The precipitation samples plot well above the GMWL. The mechanism of recharge is direct recharge. Two stalagmites (SHC-01 and SHC-02) were sampled from the cave. The first sample (SHC-01) is dated from 1012 ± 42 to 494 ± 29 yr B.P. and the second sample (SHC-02) dates between 8025 ± 38 to 6977 ± 219 yr B.P. Oxygen and carbon isotope results show that there are two climate conditions for palaeoclimate reconstruction in the Sangaw district. Conditions were generally wetter and colder during 8025 ±38 to 6977 ±219 yr B.P. than current conditions; from 1012 ± 42 to 494 ± 29 yr B.P., drier and warmer conditions prevail, more similar to today.

Keywords

Speleothems, paleoclimate, cave, Kurdistan, stable isotopes

1.Introduction

During the last few decades, speleothems (stalagmites, stalactites, and flowstones) have become an important archive for continental climate variability and a major area of palaeoclimate research (e.g. McDermott, 2004; Fairchild et al., 2006; Fleitmann and Spötl, 2008; Lachniet, 2009a). Palaeoclimate records from caves can be related to broader climate change, where they have demonstrated utility for understanding climatic and environmental change (Fairchild et al., 2006a). Speleothems can grow over thousands of years by precipitation of calcite from dripwater; their age can be determined accurately through uranium-series dating (U-Pb and U-Th). They grow at cave air temperatures that are commonly very stable throughout the year, reflecting the mean annual surface temperature outside caves. Therefore, speleothems can deliver well-dated and high-resolution records of climate variation (Wang et al., 2001, 2005, 2008; Spötl et al., 2002, 2006; Bar-Matthews et al., 2003; Fleitmann et al., 2003, 2004, 2009; Genty et al., 2003; Cheng et al., 2009; Baker and Bradley, 2010; Jex et al., 2010). The way speleothems grow makes them ideal structures to measure such proxies as annual precipitation and even temperature. Dripwater in caves can capture surface climatic patterns and changes, which in turn are archived in the speleothems via the hydrologic behavior of the drips that form speleothem laminae (Baker et al., 2000).

One region where there are numerous extensive cave systems with actively growing speloethems is the region of Iraqi Kurdistan. However, palaeoclimate reconstruction through the study of caves in this region are currently poorly developed, where the lack of resources and access limited research. The high degree of karstification is witnessed and little is known about the complexity and interaction of relevant karstification processes. Shalaii Cave is one cave in the region that has shown to have numerous speleothems that likely span much of the Holocene and possibly even earlier. Understanding this cave is a critical step forward to understanding palaeoclimate events that shaped the broader region, as it offers abundant samples that are easily recovered.

This work aims to determine palaeoclimate change using ^{18}O and ^{13}C (ratios) in the speleothems recovered and determine the controlling factors of the speleothem growth rates in the cave. In this study, a $^{230}Th/U$- dating method was used for age calculation. Supplementing data monitoring samples collected from Shalaii Cave include constructing a local meteoric water line for the area using rainwater and dripwater samples. This allows the evaluation of major, minor, and trace elements in dripwater in the wider assessment objectives. To begin this study, a description of the region, cave and surrounding geology are presented. The speleothems sampled are introduced along with the relevant climate data. Field and laboratory methods used for analysis are then presented. Results from these are given. A broader discussion on the results and conclusion are then presented.

2.Location and geological setting of the study cave

Shalaii Cave is located in the low mountainous area of the Azhdagh anticline, about 26 km to the southwest of Sangaw district and about 95 km south of Sulaimaniyah City, NE Iraq in Iraqi Kurdistan (Fig. 1). The cave lies on the northeastern end of a large, rounded sinkhole. The cave is located at 45° 17′ 45″ E and 35° 08′ 49″ N that are at an elevation of 739 m above sea level, GPS (Garmin 60 CSx with the 12 channels) was used to determine the coordinates and elevation of the cave; the deepest explored elevation of the cave is 709 m above sea level.

The geology of the area is characterized by the exposure of 12 different formations dating from the Late Eocene to Late Miocene. According to the index fossil content (*Archaias kirkukensis*, *Austrotrillina howchini*, P*eneroplis*

Thomasi and *Archias* species) around the cave (Kharajiany 2008), Shalaii Cave can be associated with the Bajawan Formation in middle Oligocene rocks, starting from 33.9 Ma (Rupelian age) to 23 Ma (Chattian age), the thickness of Bajawan Formation recorded from Shalaii village is 16 m. The formation where Shalaii Cave lies and the nearby formations, consisting mainly of massive to thickly bedded, highly jointed and fractured limestone and dolomitic limestone, is highly karstified. This is the reason behind the formation of karsts in the area, that is due to percolation of ground water through joints and fractures which in turn lead to a dissolution process.

Shalaii Cave is approximately 600 m long with a ceiling height reaching nearly 30 m; small passages in some locations are less than 1m in height. The main axis tunnel of Shalaii Cave trends in an approximate N-E direction for nearly 200 m. The cave is mostly horizontal, probably formed in the vadose zone with some areas filled with soil and collapsed rocks. The galleries in the cave are divided into two different galleries; a small gallery which is nearly 200 m away from the entrance, where the monitoring took place, and a large gallery, located away from the small gallery by a distance of 30 m, with a single passage that is extensively filled with speleothems (fossil galleries; Fig. 2). The small gallery is filled with active columns, stalactites, stalagmites and flowstones. In some parts, the concretions have reached several meters in height. The larger gallery is filled with various types of speleothems, ranging from rimstone dams, stalactites, stalagmites, columns, popcorn balls, flowstone, shelfstone and moonmilk. These passages have no running underground water flow but do have filled in water pools.

The study area climate is continental arid to semi-arid. The climatic data of the Chamchamal station for the period of 2000-2014 is used to analyze the climatic condition of the study area. The average annual rainfall of the area for the period of 2000-2014 is 463 mm. The maximum rainfall falls in January 104 mm and the minimum occurs in July 0.2 mm and August, where that month is usually a zero-rainfall month. The average minimum monthly temperature occurs in January 7.1 °C and 33.2 °C is the average maximum monthly temperature in August. Temperature higher than 40 °C commonly occurs within the study area; temperature below zero occurs as well in the winter months. The monthly average temperature for the recorded period of 2000-2014 is 20 °C. The average annual relative humidity is 42 %. The average minimum monthly relative humidity occurs in July at 20.8 %, and 67 % is the average maximum monthly relative humidity occurring in January.

3. Materials and methods

Fieldwork began in June 2014. Firstly, this included mapping and documenting the cave. The cave's dimensions, finding known entrances, while also recording the geology and geomorphology of the area, were documented. Two stalagmites samples were collected from the first gallery in Shalaii Cave and were labelled SHC-01 and SHC-02. Fig. 2 shows their location inside the cave from where the samples were collected, in addition to other monitoring stations established. SHC-01 and SHC-02 were recovered from the small gallery of the cave, about 200 m from the entrance. They were already broken when collected; it is unknown when or how exactly the stalagmites were broken. The two stalagmites samples were cut in half along their central growth axes using a MK diamond wet saw, where they were then polished to show the location of the laminae. They were packaged and posted to the Archaeology Department at the University of Reading in the United Kingdom for isotopic analysis, while the Trace Metal Isotope Geochemistry Laboratory in the University of Minnesota conducted (^{234}U-^{230}Th) dating.

The dripwater was monitored for isotopic and physiochemical analysis. Two sites were chosen in the small gallery for dripwater sampling and monitoring; the first one (site 1) is located near the location of the recovered stalagmite SHC-1. While the second one (site 2) was located near the soil hill, where the drip meter was placed away from it by nearly 3 meters. The collected dripwater in site 1 was used for isotopic composition ($\delta^{18}O$, $\delta^{2}H$) analysis and the collected dripwater in site 2 was used for alkalinity, cations, anions and trace elements analysis. The dripwater samples were collected using polyethylene funnel and bottles. The pool water samples were collected from the second large gallery for isotopic composition ($\delta^{18}O$, $\delta^{2}H$) analysis. The bottles were rinsed with dripping water before collection to minimize contamination. One sample of dripwater from the cave was collected for testing stable isotopes with polyseal cap (50 ml.) from each month starting from June 2014 to May 2015.

Rainwater samples were collected in the Chamchamal meteorological station; this included samples for $\delta^{2}H$, and $\delta^{18}O$ analysis, where water was collected during the rainy season starting from November 2014 and lasting to April 2015. For these months, samples were collected, once a month, and rainwater for each day was mixed with the samples tested to aggregate the total for the average rainfall for that month (IAEA, 1996). Rainwater samples were collected for each rain event in a bottle with a narrow head; this bottle type did not allow for evaporation of collected water that may affect the values of stable isotopes. Modern spelothem calcite deposits was collected by placing glass plates with 10 cm x 20 cm dimensions horizontally on two actively growing stalagmites on site 1 in the small gallery of the cave (Banner et al., 2007). Plates were retrieved after ten months of study.

Temperature and humidity variation of the inside and outside of the cave were monitored using Tinytag Plus 2 internal temperatures/relative humidity (TGP – 4500). One device was placed 2m away from site 1 in the small gallery from June 2014 to March 2015; it was then formatted and replaced again in the large gallery from mid-March 2015 to March 2016. A second Tinytag logger was placed in the entrance of the cave. The TGP – 4500 is a robust temperature/relative humidity logger that is contained in a waterproof case.

Caves air were monitored monthly; the cave was visited multiple times during each season in order to assess seasonal variability. Air samples were collected inside the cave from the small gallery and the second large gallery by pumping air through Tedlar Bags ESS for air composition analysis for two periods in October 2014 and April 2015. This analysis was conducted by Royal Holloway University's Earth Sciences Department. In addition, CO_2 concentration was measured in the cave air by a CO_2 meter Air CO_2ntrol 3000 and recorded monthly.

3.1 ^{234}U-^{230}Th dating

Radiogenic dating techniques are used to determine the age of speleothems. The most widely applicable is ^{230}Th - ^{234}U - ^{238}U disequilibrium dating. While uranium series dating can be used with lead for dating between 1 million and 4.5 billion years, thorium is more applicable up to 500 thousand years ago (Edwards et al., 1986). Calcite powders were milled and dissolved in nitric acid, then spiked with ^{229}Th–^{233}U–^{236}U and the Th and U were separated using anion resin columns (Asmerom et al., 2010; Beynen et al., 2017; Pollock, 2017). A ThermoFisher Scientific Neptune plus MC-ICPMS was used for dating analysis in the Minnesota University laboratory. The advantages of the (MC-ICPMS) analysis method are that they are insensitive to impurities such as organics and high precision of 0.1 - 0.4 % (Fairchild et al., 2006 b, Woodhead et al., 2006, Woodhead et al., 2012).

3.2 $\delta^{18}O$ and $\delta^{13}C$ carbonate analysis

Micro-drilling samples from the two speleothems were conducted. For the SHC-01, it was done from the top (0) cm to a depth of 31 cm down the growth axis of the stalagmite, with a total of 31 samples; for SHC-02, the samples were from the top (0) cm to 33 cm, with 33 total samples analysed. The drilled powder was transferred to a glass reaction vessel and analyzed for ^{18}O and ^{13}C stable isotopic composition on a Thermo-Finnigan Delta Plus Mass Spectrometer in the Archaeology Department at the University of Reading in the UK with procedures similar to those described in Kanner et al. (2013). The isotopic values are reported in per mil (‰) relative to Vienna Pee Dee Belemnite (VPDB).

3.3 $\delta^{18}O$ and $\delta^{2}H$ isotopes of rain and dripwater samples

Rain, pool and dripwater sample were measured using PICARRO cavity ring spectrometer L2120-I from the Archaeology Department at the University of Reading. A volume of 0.3–5 ml of sample water was equilibrated for at least eight hours with CO_2 gas; the equilibrated CO_2 gas was sampled and analyzed by a reference gas of known isotopic composition. All hydrogen and oxygen isotope values obtained through mass spectrometric analysis are reported in per ml (‰) relative to the (VSMOW).

3.4 Measurement of flowstone growth rates

The amount of calcite growth during ten months was determined by scratching the calcite growth carefully from a glass plate; this was then put in a cleaned small bowl with the bowl weighed before and after putting the calcite inside an electronic sensitive balance (OHAUS EXPLORER) in the Department of Chemistry at Sulaimani University. The plate was also weighed before and after the calcite was added. The percentages of $CaCO_3$ and $MgCO_3$ in the calcite precipitate on the glass plate were measured by an Auto Calcimeter model (XLD-MC-2) in the Department of Geology at the University of Sulaimani.

3.5 Cave air sample analysis

The cave air was analyzed using gas chromatograph at Royal Holloway's Earth Science Department using a protocol applied in Zazzeri et al. (2015). The analysis was done by an aliquot of 10 cm^3 air sample, which was taken out of Tedlar bags and injected into a flame ionized detector gas chromatograph. Later, it was heated at 240 ˚C and equipped with an 80/100 mesh, 6 ft (1.8 m) long, 1/8″ (3mm) diameter Chromosorb 102 packed column and N_2 carrier. A catalytic reactor connected to the end of the chromatographic column performed the reduction of CO_2 to CH_4; the accuracy of the measurements is 1.5 %. The GC was fitted with a flame ionization detector (FID) for CH_4 and a thermal conductivity detector (TCD) for CO_2. Standard gas mixtures were used for 3-point calibration curves to convert signals measured on the GC to concentrations (Webster et.al., 2018).

4. Results

4.1. The SHC-01 and SHC-02 stalagmite visual description

According to the above context and background, the speleothem samples (SHC-01 and SHC-02) assessed can be

described. Figure 3A, B outline the general features of the stalagmites. The stalagmites SHC-01 and SHC-02 are 33 cm and 31 cm long and 16 cm and 13 cm wide respectively. They are characterized by a columnar shape and growth that is constant in diameter. These characterizations are attributed to a slow and low dripping rate which are fed by vadose seepage flow water (McDermott et al., 2006). Visually, the laminae of the stalagmite curve at the apex then thin and trail down the sides of the stalagmite. In all cases, the curved growth morphology is interpreted to result from changes in the position of the drip location on the surface of the cave over time. The sampled speleothems, which have been recrystallized, seem more dull, massive, brownish and grainy in the middle part of them, owing to calcite mosaics, causing them to lose their acicular texture if they existed (Martín-García et al., 2009, Alonso-Zarza et al., 2011). No hiatuses can be observed in both of these samples, suggesting continual growth.

4.2 Drip rates

The drip rates were measured daily at Shalaii Cave starting in July 2014 and ending May 2015 (Fig. 4A). The coarse resolution of the datasets precludes precise characterization of individual drip collections' temporal behavior. Therefore, the discussion focuses on spatial variability and the time series datasets are used to characterize the flow regime of the individual drip site. Dripwater demonstrates that the drip site maintains a given flow throughout the year, with the average drip rates ranging between 4408 drips/day – 29199 drips/day, with the lowest drip rates in summer months and the highest in winter months, reflecting seasonal recharge to the aquifer. The relationship between precipitation (the system input) and dripwater flow (the system output; Fig. 4B) helps determine the effect of precipitation on dripwater flow. It can be seen that dripwater continues to drip during the summer, although there is no precipitation source to recharge it, meaning that the karst has a large storage capacity during the winter season. Drip rate in Shalaii Cave responds to precipitation change.

4.3 Cave air content and direction, temperature and humidity

The results of cave air chemistry are tabulated in Table 1. The methane source in cave air is represented by the atmosphere, soil air, cave air and ground air. Ground air consists of CO_2-rich air permeating the unsaturated zone (Atkinson, 1977 a). Because of density has driven seasonal advection of air through the bedrock, it acts both as a source and a sink for the gas reservoir in cave air. Cave air is linked to the background atmosphere via two pathways. One of them passes through the soil zone and forms the ground air source for cave air; the other is a direct link representing ventilation through cave entrances.

Shalaii Cave has one entrance, detected by using a smoker continuously during the period of the study to determine the direction of air circulation. It was observed that the smoker did not change and stayed constant; this indicates that Shalaii Cave has no air circulation since it has one entrance. Thus, ground air is depleted in methane due to the (1) exchange with methane depleted soil air and (2) oxidation of incoming atmospheric CH_4 in the cave reservoir in the summer advection mode. In the winter advection mode, methane depleted ground air is exhaled either directly to the atmosphere through cave entrances, or by permeation through the soil zone, providing further opportunities for methane stripping.

The temperature readings of the Tinytag device range from -40 °C to +85 °C, while the relative humidity readings range from 0-100 % with a reading resolution accuracy of 0.01°C. The logger was calibrated to measure

readings every 12 hours, the data were retrieved at one-month intervals. A drip meter Tintag tool (STALAGMITE MR3) was fixed on an active stalagmite in site 2 in the small gallery to measure the rate of the fallen dripwater. The logger was calibrated to measure readings every 12 hours during the whole period of the research.

Ten months worth of temperature measurements, taken over 2015, show that recent temperature inside the studied cave is stable throughout the research period. For Shalaii Cave, temperature at the entrance point show variation, with the average being 17.1 °C, minimum 13.0 °C, and maximum 22.3 °C, which are indicated in Fig. 5A. This variation means that a response to surface temperature changes above the cave is evident. On the other hand, temperature in the small gallery and the large one does not response directly to surface temperature changes, where the average outside air temperature was 20.5 ºC, with average cave temperature at 20.18 °C, minimum was 20.15 °C, and maximum 20.19 °C, as shown in Fig. 5A. This suggest that the epikarst can store some of the surface heat. Rock and soil cover can act as heat insulators, preventing substantial temperature variations. Such thermal insulation creates relatively stable temperature changes in Shalaii Cave. However, the temperature measurements obtained over the ten months of monitoring show that the cave entrance opening does not impact greatly temperature variations inside the cave.

Measurements of relative humidity for ten months show that the relative humidity inside the cave is stable throughout the research period. For the Shalaii Cave, the relative humidity at the entrance point, generally show variation around an average of 66.6 %, with a minimum of 33.6 % and maximum at 95.8 %. This means that there is a response to surface humidity changes. While the temperature in the first gallery does not respond directly to surface humidity changes, where the average outside air relative humidity is 40 %, average cave relative humidity was 100 %, with both minimum and maximum 100 % being the same (Fig. 5B).

4.4 Calcite growth and cave CO_2 concentration

Calcite growth at site 1 reflects a seasonal growth pattern in which higher cave air CO_2 concentrations inhibit CO_2 degassing from cave dripwater and thus inhibit calcite precipitation. This process is driven by varying temperature gradient between surface air and cave air, which drives the ventilation of caves (Banner et al., 2007). The average cave air pCO_2 is 596 ppm; in Shalaii Cave air pCO_2 (Fig. 5C) rises in mid-January, reaching winter values of 756 ppm and then falling to less than 484 ppm in mid–September, which is nearly atmospheric. The control on cave air pCO_2 is complex; in the winter there is a rise in cave air pCO_2, which is primarily a result of reversals in chimney ventilation driven by temperature being in contrast between the cave interior and exterior, with additional transient effects caused by synoptic scale atmospheric pressure and wind conditions (Mattey et al., 2008). In Shalaii Cave, site1's modern calcite deposition on the glass plate was (1.3312 mg), which was 0.132 mm during nine months of monitoring. By using a Calcimeter for analyzing the content of modern calcite, it appears that 100 % of its content is calcite.

4.5 ^{2}H and ^{18}O of the dripwater and precipitation

The results of ^{2}H and ^{18}O of dripwater samples are shown in the table 2; the average isotopic composition of the dripwater samples is -5.611 and 42.102 ‰ for the $\delta^{18}O$ and $\delta^{2}H$ respectively. This verifies that the dripwater of Shalaii Cave originates from a meteoric origin. The differences in ($\delta^{2}H$ and $\delta^{18}O$) compositions between the analyzed

samples are not large, suggesting that the cave has little evaporation. The previous stable isotope data of precipitation data are not available. Consequently, the obtained results of this study during the 2014- 2015 rainy season in the area of interest would be adopted and presented here. The rain water in the beginning and the end season is enriched in δ^2H and $\delta^{18}O$, that is due to the low intensity of rainfall generally occurring in high temperature and low humidity conditions than rainfall events during the rest of the year (Gat, 1996) (Fig. 6A). Table 2 shows the range of the isotopic values during the entire rainy season (2014-2015), which is between-6.1 ‰ and -4.01 ‰ for $\delta^{18}O$ and between -48 ‰ and -34.7 ‰. for δ^2H. The relation between$\delta^{18}O$ and δ^2H of the rainwater is a function of the amount of rainfall and the intensively of rainfall events, usually heavy rainfall per event, with a greater slope with a high d-excess, whereas light rain showers form a trend along the evaporation line with less slope and low d-excess. These deviations from the GMWL are a consequence of the evaporation processes occurring during the descent of clouds to the ground (Gat 1996; Gat and Dansgaard 1972; Gat and Carmi 1970).

Generally, rainwater $\delta^{18}O$ values at a specific location vary due to temperature change, variation of rainfall, fluctuations in the source of the rainwater or cloud track (Rozanski et al., 1993). The average $\delta^{18}O$ and δ^2H compositions of the dripwater are slightly lighter compared to the average $\delta^{18}O$ and δ^2H compositions of the rainwater (Fig. 6B). This slight increase in rainwater δ values is possible due to evaporation of precipitated meteoric water from the sampling bottle or more infiltration of water in the colder period of the year. A minimum value of $\delta^{18}O$ in dripwater was in January 2015; this larger drop corresponds with a decrease in temperature or with an increase in rainfall amount. The summer season is most probably responsible for the slightly more positive $\delta^{18}O$ and δ^2H values in the dripwaters. The $\delta^{18}O$ and δ^2H composition of the dripwater display almost slight variations throughout the year except November and December, where they became more positive due to evaporation or mixing, indicating that the water residence time is sufficiently long to homogenize its isotopic composition.

4.6 The $\delta^{18}O$ and $\delta^{13}C$ carbonate record from the stalagmites

The $\delta^{18}O$ values of SHC-01 ranges from -7.6 ‰ to -5.8 ‰, with an average of -6.7 ‰. While the $\delta^{13}C$ values range from -10.1 ‰ to -7.8 ‰, with an average of -9.1 ‰. Fig.7A indicates that stalagmites in the inner part of Shalaii Cave were deposited in or very close to isotopic equilibrium because the inside of Shalaii Cave has a high relative humidity of 100 %. The $\delta^{18}O$ values SHC-02 range from -6.3 ‰ to -4.9 ‰, with an average of -5.4 ‰. While the $\delta^{13}C$ values range from -11.6 ‰ to -9.1 ‰, with an average of -10.1 ‰ (Fig.7B).

4.7 ^{234}U-^{230}Th chronology

Speleothems are well suited for the establishment of precise and accurate age models, which are essential to determining environmental information stored in them. In fact, their excellent dating eligibility and their dating range is one of the major strengths compared to other climate archives and explains, to a large extent, their growing importance and popularity in paleoclimate research. Results of the age dating are presented in table. 3. The SHC-01 stalagmite growth ranged from nearly 1012.00 ±42 yr B.P. to 494.00 ±29 yr B.P. (Late Holocene). The SHC-02 stalagmite growth ranged from 8025 ±38 yr B.P. to 6977 ±219 yr B.P. (Early Holocene).

5. Discussion

5.1 δ^2H and $\delta^{18}O$ relationships

The isotopic data plotted on the GMWL and a local meteoric water line, obtained and named the Sangaw Meteoric Water Line (SMWL), represents the ^2H and ^{18}O relation in the area of interest, has the following formula:

$$\delta^2H = 8.0331 \times \delta^{18}O + 19.8 \text{ .....(1)}$$

This line is an average of multiple global meteoric water lines, which differ from the Sangaw line due to varying climatic and geographic parameters. Both the SMWL and the GMWL are presented (Fig. 8), which shows the relationship of deuterium composition (δ^2H) and oxygen–18 composition ($\delta^{18}O$) based on five samples of rain. On this plot, the data define a clear linear trend that represents the local meteoric water line for Sangaw (SMWL) region during the rainy season (from November to March) in 2014-2015. The slope (3.0034) and intercept (-25.25) of the dripwater are both higher than that of the global meteoric water line (GMWL, 8 and 10; Craig, 1961) because they display about 50 % humidity, where the vapor is strongly depleted. The precipitation plots are well above the GMWL.

5.2 $\delta^{13}C$ variations in cave air

The $\delta^{13}C$ variations in cave air methane provide considerable insight into the nature of the gas exchange between the atmospheric and ground air methane reservoirs. Methane abundances in cave air are uncorrelated with soil zone methane but show an inverse relationship to the ventilation controlled seasonal cycles shown by CO_2. Cave air CH_4 abundances are strongly inversely correlated with $\delta^{13}C$ (Table 1). The cave air data patterns, characterised by elevated CH_4 mixing ratios with δ^{13} CH_4 values, indicate intermittent presence of a biogenic input from the above soil's organic matter. The isotopic signature of microbial oxidation is present in cave air samples which were taken when the cave was ventilating in both summer and winter modes. In winter, CO_2-rich ground air advects out of the caves into the atmosphere that is strongly depleted in methane, but summer ventilation displaces cave air with a CH_4-rich background atmosphere, restoring methane levels to around only the atmospheric background concentration.

5.3 SHC-01 anomalies in proxy record

The stable oxygen records in SHC-01 tend to be more positive than in SHC-02; this likely indicates climate shifted toward drier conditions in the later sample SHC-02 (Marsh et al., 2018; Talbot, 1990). While accounting for error, Figure 9A shows the periods which the $\delta^{18}O$ is above the average value and are between 494 to 527.4, 561 to 644, 678 to 695, 812, 912, 979 and 995, from drier and warmer winters. The periods below the average value are between 527 to 561, 644 to 661, 711 to 812, 862, 895 and 945 demonstrate likely drier winters (Fig. 9A). Changes in the Earth's orbit relative to the sun are the most significant climate-force in the mid to late Holocene; with the $\delta^{18}O$ variations responding to solar insolation impact that lead to gradually decreasing precipitation (Fairchild and Baker, 2012). In the context of the southerly moving ITCZ (Intertropical Convergence Zone; Huang et al., 2001), the Afro-Asian summer monsoon weakened greatly, causing aridity in subtropical Africa and Asia and in Central America. While the $\delta^{13}C$ tend to be more negative than the $\delta^{13}C$ of SHC-02, this is related to several different effects including: (1) vegetation density (more dense vegetation = more negative values), due to the increased anthropogenic impact on land cover and intensification of agriculture, (2) recharge conditions (infiltrated rainfall may fully

equilibrate with soil CO_2 at times of low rainfall), (3) drip rate, and (4) CO_2 degassing inside the cave. The palaeoclimate for the early and mid-Holocene in the Sangaw area appears to have been generally wetter and cooler than in the late Holocene.

5.4 SHC-02 anomalies in proxy record

The stable oxygen record is interpreted to reflect the precipitation amount, meaning that increased precipitation leads to more depleted values of $\delta^{18}O$ in the stalagmite and vice versa (Fig. 9B). Four periods where the $\delta^{18}O$ abruptly decrease away from the average values line occur in the stalagmite from 6977 to 7403 yr B.P., from 7436 to 7632 yr B.P., from 7731 to 7796 yr B.P. and from 7862 to 8025 yr B.P., which are interpreted as anomalies in the record. The isotope proxies show concurrent large amplitude changes and reflect cold and wet winter periods. The thick calcite annual layers suggest that a high amount of water was dripping on the stalagmite during that period (Fig. 8B). Therefore, this period is interpreted as an anomaly, reflecting wet and cold winters since the oxygen isotope values of the stalagmite (early Holocene) are more negative. This may be related to the 8.2 kyr B.P. event which occurred due to a large meltwater pulse from the final collapse of the ice sheets, causing the climate to become colder and less humid, and the so-called oceanic source effect (Rohling and Palike, 2005).

The latter effect is related to changes in the oxygen isotopic composition of seawater, in this case the Mediterranean was generally more negative during the early and mid-Holocene due to higher discharge of isotopically depleted Nile water, which is why the formation of sapropels layers at this time are evident (Meyers and Arnaboldi, 2008). These generally higher precipitation in the Eastern Mediterranean likely affected Shalaii Cave. The stable carbon isotope record is interpreted to reflect changes in biological activity, that is vegetation changes a result of both climate variability and changes in the intensity of human activities. The carbon isotope signal is very noteworthy, since the early Holocene values are actually more positive, which could be related to several different effects including: (1) vegetation density (less dense vegetation = more positive values), (2) recharge conditions (infiltrated rainfall may not fully equilibrate with soil CO_2 at times of very high rainfall) and (3) drip rate and CO_2 degassing inside the cave.

6. Conclusions

Based on different investigation methods, we indicate that there is no air circulation inside the cave as the cave has only one entrance and a thick epikarst zone, which classifies Shalaii Cave to be a closed system cave. The average CO_2 concentration is 598 ppm, the source of the methane in the air sample content is probably from underground. The average drip rates are between 4408 drips/day – 29199 drips/ day, with the lowest drip rates in summer and the highest in winter. This indicates that the type of flow is seasonal. The values $\delta^{18}O$ and $\delta^{2}H$ of rainfall are influenced by the temperature effect, usually increasing during the summer months. The precipitation plots are well above the GMWL. The $\delta^{18}O$ and $\delta^{2}H$ of the dripwater remain constant, due to a long residence time of the water in the epikarst and a well-mixed aquifer. The cave air data patterns, characterised by elevated CH_4 mixing ratios with $\delta^{13}CH_4$ values, provide evidence of the intermittent presence of biogenic input from the above soil's organic matter.

The Uranium-Thorium analysis indicates that SHC-01 is late Holocene (1012 ± 42 yr B.P. to 494 ± 29 yr B.P.) and is younger than SHC-02 (early Holocene; 8025 ± 38 yr B.P. to 6977 ± 219 yr B.P.). Palaeoclimate

reconstruction of the two main climate conditions can be identified in Sangaw district during 8025 ± 38 yr B.P. to 6977 ±219 kyr yr B.P., with the conditions mainly being wetter than current conditions, while during 1012 ± 42 yr B.P. to 494 ± 29 yr B.P. the conditions were drier in the district. From the speleothems, there is local evidence of change in precipitation amounts, with rapid shifts from wetter conditions to developing aridity between the early/mid to late Holocene.

Acknowledgments

The authors show their appreciation to Dr. Dominik Flietmann from Reading University, for his encouragement, guidance, and support in speleothem analysis. The authors greatly appreciate Dr. Ian Fairchild from Birmingham University and Dr. Claire Smith and Arnoud Boom from Leicester University for their excellent assistance, advice and the valuable references they provided throughout this work. We provide our appreciation to the University of Minnesota Laboratory run by Professor Larry Edwards and Birmingham University's Department of Earth Sciences. We would like to thank the Sulaimaniyah Meteorological Station for their assistance in obtaining meteorological data.

References

Abrantes, E. A., Bellini. B. C., Bernardo, A. N., Fernandes, L. H., Mendonça, M. C., Oliveira, E. P., Queiroz, G. C., Sautter, K. D., Silveira, T. C. and Zeppelini, D., 2010. Synthesis of Brazilian Collembola: An update to the species list. Zootaxa 2388: 1- 22.

- Alonso-Zarza, A. M., Martín-Pérez, A., Martín-García, R., Gil-Peña, I., Meléndez, A., Martínez-Flores, E., Hellstrom, J. and Muñoz-Barco, P., 2011. Structural and host rock controls on the distribution, morphology and mineralogy of speleothems in the Castañar Cave (Spain). Geol Mag. 148, 2, 211-225. https://doi.org/10.1017/S0016756810000506

Asmerom, Y., Polyak, V. and Burns, S. ,2010. Variable winter moisture in the southwestern United States linked to rapid glacial climate shifts. Nat Geosci. 3, 114–117. https://doi.org/10.1038/ngeo754

Atkinson, T. C. ,1977. Carbon dioxide in atmosphere of unsaturated zone - important control of groundwater hardness in limestones. J Hydrol. 35**,** 111-123. https://doi.org/10.1016/0022-1694(77)90080-4

Baker, A. and Bradley, C., 2010. Modern stalagmite $\delta^{18}O$: instrumental calibration and forward modelling. Glob Planet Change. 71, 201-206. https://doi.org/10.1016/j.gloplacha.2009.05.002

Baker, A., Genty, D. and Fairchild, I. J., 2000. Hydrological characterisation of stalagmite dripwaters at Grotte de Villars, Dordogne, by the analysis of inorganic species and luminescent organic matter. Hydrol Earth Syst Sci. 4, 439-449. https://doi.org/10.5194/hess-4-439-2000

Banner, J.L., Guilfoyle, A., James, E.W., Stern, L.A. and Musgrove, M., 2007. Seasonal variations in modern speleothem calcite growth in central Texas, USA. J Sediment Res, *77*, 615-622. https://doi.org/10.2110/jsr.2007.065

Bar-Matthews, M., Ayalon, A., Matthews, A., Sass, E. and Halicz, L., 1996. Carbon and oxygen isotope study of the active water-carbonate system in a karstic Mediterranean cave: Implications for paleoclimate research in semiarid regions. Geochim Cosmochi Acta, vol. 60, 337-347. https://doi.org/10.1016/0016-7037(95)00395-9

Bar-Matthews, M., Ayalon, A., Gilmour, M., Matthews, A., Hawkesworth, C.J., 2003. Sea - land oxygen isotopic relationships from planktonic foraminifera and speleothems in the Eastern Mediterranean region and their implication for paleorainfall during interglacial intervals. Geochim Cosmochi Acta. 67, 3181-3199. DOI:10.1016/S0016-7037(02)01031-1

Cheng, H., Edwards, R., L., Broecker, W. S., Denton, G. H., Kong, X. G., Wang, Y. J., Zhang, R. and Wang, X. F. 2009. Ice age terminations. Science, 326, 248-252. DOI: 10.1126/science.1177840

Edwards, R. L., Chen, J. H., Wasserburg, G. J., 1986. ^{238}U-^{234}U-^{230}Th-^{232}Th systematics and the precise measurement of time over the past 500,000 years. Earth Planet Sci Lett, 81, 175-192. https://doi.org/10.1016/0012-821X(87)90154-3

Fairchild, I. J. and Baker, A. 2012. Speleothem Science from process to past environments. Willey- Blackwell, London. 337 p.

Fairchild, I.J., Smith, C.L., Baker, A., Fuller, L., Spötl, C., Mattey, D., McDermott, F., 2006a. Modification and preservation of environmental signals in speleothems. Earth-Science Reviews, 75, 105-153. https://doi.org/10.1016/j.earscirev.2005.08.003

Fleitmann, D. and Spötl, C., 2008, Advances in speleothem research. Pages news. vol.16, no. 3.

Fleitmann, D., Burns, S. J., Mudelsee, M., Neff, U., Kramers, J., Mangini, A. and Matter, A., 2003a. Holocene forcing of the Indian monsoon recorded in a stalagmite from Southern Oman. Science, 300, 1737-1739. DOI:10.1126/science.1083130

Fleitmann, D., Burns, S. J., Neff, U., Mangini, A. and Matter, A., 2003b. Changing moisture sources over the last 330,000 years in Northern Oman from fluid-inclusion evidence in speleothems. QUATERNARY RES, 60, 223-232. https://doi.org/10.1016/S0033-5894(03)00086-3

Fleitmann, D., Burns, S. J., Neff, U., Mudelsee, M., Mangini, A., and Matter, A., 2004. Palaeoclimatic interpretation of high-resolution oxygen isotope profiles derived from annually laminated speleothems from Southern Oman. Quaternary Sci Rev, 23, 935-945. https://doi.org/10.1016/j.quascirev.2003.06.019

Fleitmann, D., Cheng, H., Badertscher, S., Edwards, R. L., Mudelsee, M., Gokturk, O. M., Fankhauser, A., Pickering, R., Raible, C. C., Matter, A., Kramers, J. and Tuysuz, O., 2009. Timing and climatic impact of Greenland interstadials recorded in stalagmites from northern Turkey. Geophys Res Lett, 36, L19707 https://doi.org/10.1029/2009GL040050

Frumkin, A., Ford, D. C., and Schwarcz, H. P., 2000. Paleoclimate and vegetation of the last glacial cycles in Jerusalem from a speleothem record. Global Biogeochem Cycles,14, 863-870. https://doi.org/10.1029/1999GB001245

Gat, J. R., 1996. Oxygen and hydrogen isotopes in the hydrologic cycle. Annu Rev Earth Planet Sci, 24, 225-262. https://doi.org/10.1029/1999GB001245

Gat, J. R. and Carmi, I., 1970. Evolution of the isotopic composition of atmospheric waters in the Mediterranean Sea area. J Geophys Res, 75, 3039-3048. https://doi.org/10.1029/JC075i015p03039

Gat, J. R. and Dansgaard, W., 1972. Stable isotope survey of the fresh water occurrences in Israel and the Northern Jordan Rift Valley. J Hydrol, 16, 177-211. https://doi.org/10.1016/0022-1694(72)90052-2

Genty, D., Blamart, D., Ouahdi, R., Gilmour, M., Baker, A., Jouzel, J., Van-Exter, S., 2003. Precise dating of Dansgaard-Oeschger climate oscillations in western Europe from stalagmite data, Nature, 421, 833-837. DOI:10.1038/nature01391

Hendy, C. H., 1971. Isotopic geochemistry of speleothems calculation of effects of different modes of formation on isotopic composition of speleothems and their applicability as paleoclimatic indicators. Geochim Cosmochi Acta, 35, 801. DOI: 10.1016/0016-7037(71)90127-X

Huang, Y., Fairchild, I. J., Borsato, A., Frisia, S., Cassidy, N. J., Mcdermott, F. and Hawkesworth, C. J., 2001. Seasonal Variations in Sr, Mg and P in modern speleothems (Grotta Di Ernesto, Italy). Chem Geol, 175, 429-448. https://doi.org/10.1016/S0009-2541(00)00337-5

IAEA - International Atomic Energy Agency, 1996. Statistical treatment of data on environmental isotopes in precipitation. Technical reports series No. 331. Vienna.

Jex, C.N., Baker, A., Fairchild, I. J., Eastwood, W.J., Leng, M.J., Sloane, H.J., Thomas, L., Bekaroğlu, E., 2010. Calibration of speleothem $\delta^{18}O$ with instrumental climate records from Turkey. Glob Planet Change,71, 207-217. https://doi.org/10.1016/j.gloplacha.2009.08.004

Kanner, L.C., Burns, S.J., Cheng, H., Edwards, R.L. and Vuille, M., 2013. High-resolution variability of the South American summer monsoon over the last seven millennia: insights from a speleothem record from the central Peruvian Andes. Quat Sci Rev, 75, 1-10. https://doi.org/10.1016/j.quascirev.2013.05.008

Kharajiany S. O. A., 2008. Sedimentary facies of Oligocene rock units in Ashdagh mountain- Sangaw district-Kurdistan region-NE Iraq, Unpublished MSc thesis, College of Science, University of Sulaimani.

Kharajiany S. O. A., 2014. Occurrence of Early and Middle Miocene rocks (Euphrates, Dhiban And Jeribe Formations) In Ashdagh Mountain, Sangaw Area, Sulaimanyah Vicinity, NE Iraq. Iraqi Bulletin of Geology and Mining, 10, 1, 21-39.

Lachniet, M. S., 2009. Climatic and environmental controls on speleothem oxygen-isotope values. Quat Sci Rev, 28, 412-432. https://doi.org/10.1016/j.quascirev.2008.10.021

Leng, M. J., 2005. Isotopes in paleoenvironmental research. Springer. Dordrecht, the Netherlands. 307p.

Marsh, A., Fleitmann, D., Al-Manmi, D. A. M., Altaweel, M., Wengrow, D., & Carter, R., 2018. Mid- to late-Holocene archaeology, environment and climate in the northeast Kurdistan region of Iraq. *The Holocene*, *28*(6), 955–967. https://doi.org/10.1177/0959683617752843

Martín-García, R., Alonso-Zarza, A. M. and Martín-Pérez, A., 209. Loss of primary texture and geochemical signatures in speleothems due to diagenesis: Evidences from Castañar Cave, Spain. Sediment. Geol.**,** 221, 141-149. DOI: 10.1016/j.sedgeo.2009.09.007

Mcdermott, F., 2004. Paleoclimate reconstruction from stable isotope variations in speleothems: A review. Quat Sci Rev, 23, 901-918. DOI: 10.1016/j.quascirev.2003.06.021

Mcdermott, F., Schwarcz, H. P. and Rowe, P. J., 2006. Isotopes in Speleothems. In: Leng, M. J. (Ed.), Isotopes in paleoenvironmental Research. Heidelberg: Springer.

Meyers, P and Arnaboldi, M., 2008. Palaeoceanographic implications of nitrogen and organic carbon excursions in mid-Pleistocene sapropels from the Tyrrhenian and Levantine basins, Med Sea. Palaeogeogr Palaeoclimatol Palaeoecol, 266, 112-118. https://doi.org/10.1016/j.palaeo.2008.03.018

Plagnes, V., Causse, C., Genty, D., Paterne, M. and Blamart, D., 2002. A discontinuous climatic record from 187 to 74 ka from a speleothem of the Clamouse Cave (south of France). Earth Planet Sci Lett, 201, 87-103. https://doi.org/10.1016/S0012-821X(02)00674-X

Pollock, A.L., van Beynen, P.E., DeLong, K.L., Polyak, V. and Asmerom, Y., 2017. A speleothem-based mid-Holocene precipitation reconstruction for West-Central Florida. The Holocene, 27,7, 987-996. https://doi.org/10.1177/0959683616678463

Pourmand, A, Tissot, F, Arienzo, M., and Sharifi, A., 2014. Introducing a comprehensive data reduction and uncertainty propagation algorithm for U-Th geochronometry with Extraction Chromatography and isotope dilution MC-ICP-MS. GEOSTAND GEOANAL RES, 38, 2, 129-148. https://doi.org/10.1111/j.1751-908X.2013.00266.x

Rohling, E.J. and Palike, H., 2005. Centennial- scale climate cooling with a sudden cold event around 8200 years ago. Nature, 434, 975-979. DOI:0.1038/nature03421

Rozanski, K., Araguas, L. and Gonfiantini, R., 1993. Isotopic patterns in modern precipitation. In*:* Swart, P. K., Lohmann, K. C., Mckenzie, J. & Savin, S. (eds.), Climate Change in Continental Isotopic Records. Washington, D.C.: American Geophysical Union. https://doi.org/10.1029/GM078p0001

Spötl, C. and Mangini, A., 2002. Stalagmite from the Austrian Alps reveals Dansgaard-Oeschger events during isotope stage 3: Implications for the absolute chronology of Greenland ice cores, Earth Planet Sci Lett, 203, 507-518. https://doi.org/10.1016/S0012-821X(02)00837-3

Spötl, C. and Mangini, A., 2006. U-Th age constraints on the absence of ice in the central Inn Valley (eastern Alps, Austria) during Marine Isotope Stages 5c to 5a. QUATERNARY RES, vol. 66, 167-175. https://doi.org/10.1016/j.yqres.2006.03.002.

Talbot, M. R., 1990. A review of the palaeohydrological interpretation of carbon and oxygen isotopic ratios in primary lacustrine carbonates. Chem. Geol.: Isotope Geoscience Section, 80(4), 261–279. https://doi.org/10.1016/0168-9622(90)90009-2

Van Beynen, P., Polk, J.S., Asmerom, Y. and Polyak, V., 2017. Late Pleistocene and mid-Holocene climate change derived from a Florida speleothem. Quat Int, 449, 75-82. https://doi.org/10.1016/j.quaint.2017.05.008

Wang, Y. J., Cheng, H., Edwards, R. L., An, Z. S., Wu, J. Y., Shen, C. C. and Dorale, J. A., 2001. A high-resolution absolute-dated Late Pleistocene monsoon record from Hulu Cave, China. Science, 294, 2345-2348. DOI: 10.1126/science.1064618

Wang, Y. J., Cheng, H., Edwards, R. L., Kong, X. G., Shao, X. H., Chen, S. T., Wu, J. Y., Jiang, X. Y., Wang, X. F. and An, Z. S., 2008. Millennial- and orbital-scale changes in the East Asian monsoon over the past 224,000 years. Nature, 451, 1090-1093. DOI: 10.1038/nature06692

Wang, Y., Cheng, H., Edwards, R. L., He, Y., Kong, X., An, Z., Wu, J., Kelly, M. J., Dykoski, C. A. and Li, X., 2005. The Holocene Asian Monsoon: Links to Solar changes and North Atlantic Climate. Science, 308, 5723, 854–857. DOI: 10.1126/science.1106296

Webster, K.D., Drobniak, A., Etiope, G., Mastalerz, M., Sauer, P.E. and Schimmelmann, A., 2018. Subterranean karst environments as a global sink for atmospheric methane. Earth Planet. Sci. Lett., 485, 9-18.

White, W. B., 2006. Fifty years of karst hydrology and hydrogeology: 1953-2003. In: Harmon, R.S. and Wicks, C, (ed.) prespectives on karst geomorphology, Hydrology and Geochemistry- A tribute volume to Derek C, Ford and William B, White. Geological Society of America Special Paper, 404, 139-152. DOI: 10.1130/2006.2404(12)

Woodhead, J., Hellstrom, J., Maas, R., Drysdale, R., Zanchetta, G., Devine, P., Taylor, E., 2006. U-Pb geochronology of speleothems by MC-ICPMS. Quat Geochronol, 1, 208-221. https://doi.org/10.1016/j.quageo.2006.08.002

Woodhead, J., Hellstrom, J., Pickering, R., Drysdale, R., Paul, B. and Bajo, P., 2012. U and Pb variability in older speleothems and strategies for their chronology. Quat Geochronol,14, 105-113. https://doi.org/10.1016/j.quageo.2012.02.028

Yonge, C. J., Ford, D. C., Gray, J. and Schwarcz, H. P., 1985. Stable isotope studies of cave seepage water. Chem Geol Isotope Geoscience Section, 58, 97-105. https://doi.org/10.1016/0168-9622(85)90030-2

Zazzeri, G., Lowry, D., Fisher, R. E., France, J. L., Lanoisellé, M., & Nisbet, E. G., 2015. Plume mapping and isotopic characterisation of anthropogenic methane sources. Atmos Environ, 110, 151–162. https://doi.org/10.1016/j.atmosenv.2015.03.029

Table. 1 Air contents of Shalaii Cave

Sample date	Location	CH_4 (ppm)	$\delta^{13}CH_4$ (per mil)	H_2O (%)
Oct.2014	Large Gallery	1.14	-56.3	0
Apr.2015	Small Gallery	0.22	-30.9	0.87
Apr.2015	Large Gallery	0.24	-33.8	0.88

Table. 2 The ($\delta^{18}O$ and $\delta^{2}H$) compositions of the dripwater and rainfall of the study area

Sample Date	$\delta^{18}O$ (‰)	$\delta^{2}H$ (‰)	$\delta^{18}O$ SD	$\delta^{2}H$ SD	$\delta^{18}O$ (‰)	$\delta^{2}H$ (‰)	$\delta^{18}O$ SD	$\delta^{2}H$ SD
	Dripwater				Rainfall			
Jun. 2014	-5.97	-43.3	0.12	1.39	-4.5	-36.4	0.17	0.77
Jul.2014	-5.9	-42.2	0.06	0.32	-4.0	-34.7	0.12	1.17
Aug.2014	-5.8	-42.1	0.07	0.32	-5.0	-38.3	0.13	1.19
Sept.2014	-5.7	-42.0	0.08	0.28	-6.1	-48.1	0.18	1.33
Oct.2014	-5.5	-42.5	0.14	0.64	-4.7	-43.2	0.1	1.12
Nov.2014	-5.3	-39.9	0.2	0.56	---	---	---	---
Dec.2014	-5.4	-41.0	0.1	0.59	---	---	---	---
Jan.2015	-5.7	-43.3	0.13	1.13	---	---	---	---
Feb.2015	-5.7	-42.9	0.08	0.54	---	---	---	---
Mar.2015	-5.5	-42.1	0.07	0.52	---	---	---	---
Apr.2015	-5.4	-42.0	0.08	0.54	---	---	---	---

Table. 3 Results of the SHC-01 and SHC-02, U-TH dating, $\delta^{18}O$, $\delta^{13}C$ versus depth

Stalagmite SHC- 01				Stalagmite SHC-02			
$\delta^{13}C$ (‰VPDB)	$\delta^{18}O$ (‰VPDB)	Depth from top (cm)	Years B.P. (B.P.=1950)	$\delta^{13}C$ (‰VPDB)	$\delta^{18}O$ (‰VPDB)	Depth from top (cm)	Years B.P. (B.P.=1950)
-9.7	-4.9	0	494.00±29	-8.7	-6.8	1	6977±38
-10.4	-5.0	1	511	-8.7	-6.5	2	7010
-10.3	-5.4	2	527	-9.8	-6.5	3	7043
-10.5	-6.1	3	544	-8.3	-6.6	4	7075
-9.4	-5.3	4	561	-9.6	-6.4	5	7108
-10.3	-5.2	5	578	-8.0	-6.5	6	7141
-11.2	-5.6	6	594	-9.1	-7.0	7	7174
-10.3	-5.4	7	611	-9.1	-7.0	8	7206
-10.2	-5.5	8	628	-10.0	-7.1	9	7239
-10.3	-5.7	9	644	-9.5	-7.1	10	7272
-11.5	-6.0	10	661	-9.1	-7.1	11	7305
-9.1	-5.2	11	678	-9.6	-6.2	12	7337
-928	-5.2	12	695	-9.1	-6.9	13	7370
-11.3	-5.7	13	711	-8.5	-6.2	14	7403
-11.6	-6.1	14	728	-8.8	-6.0	15	7436
-10.9	-6.3	15	745	-10.1	-6.7	16	7468
-9.8	-6.1	16	761	-8.8	-6.4	17	7501
-9.9	-6.1	17	778	-8.9	-6.9	18	7534
-10.1	-6.3	18	795	-7.8	-6.2	19	7567
-10.2	-5.8	19	812	-7.9	-6.6	20	7600
-9.9	-5.4	20	828	-8.2	-6.2	21	7632
-10.2	-6.3	21	845	-8.0	-5.8	22	7665
-10.2	-5.6	22	862	-8.5	-6.0	23	7698
-10.4	-6.3	23	878	-9.0	-6.3	24	7731
-10.2	-5.2	24	895	-9.3	-7.6	25	7763
-9.3	-5.6	25	912	-8.8	-6.4	26	7796
-9.6	-5.5	26	929	-10.0	-5.8	27	7829
-10.5	-6.3	27	945	-8.4	-6.6	28	7862
-10.3	-5.3	28	962	-8.4	-6.5	29	7894
-10.1	-5.6	29	979	-9.6	-6.6	30	7927
-9.7	-5.1	30	995	-9.5	-6.6	31	7960
-10.9	-5.8	31	1012.0±42	-9.1	-6.5	32	7993
				-8.6	-6.5	33	8025±219

Highlights

- Analysis of speleothems is significant for paleoclimate determination.
- This paper presents new data on cave monitoring from Kurdistan Province of Iraq**.**
- Stable isotopes, and cave parameters integrated to understand behavior of the cave.
- Carbon and oxygen isotopic values are useful for climatic proxies.
- Uranium - Thorium dating is a good tool for age determination of the speleothems.

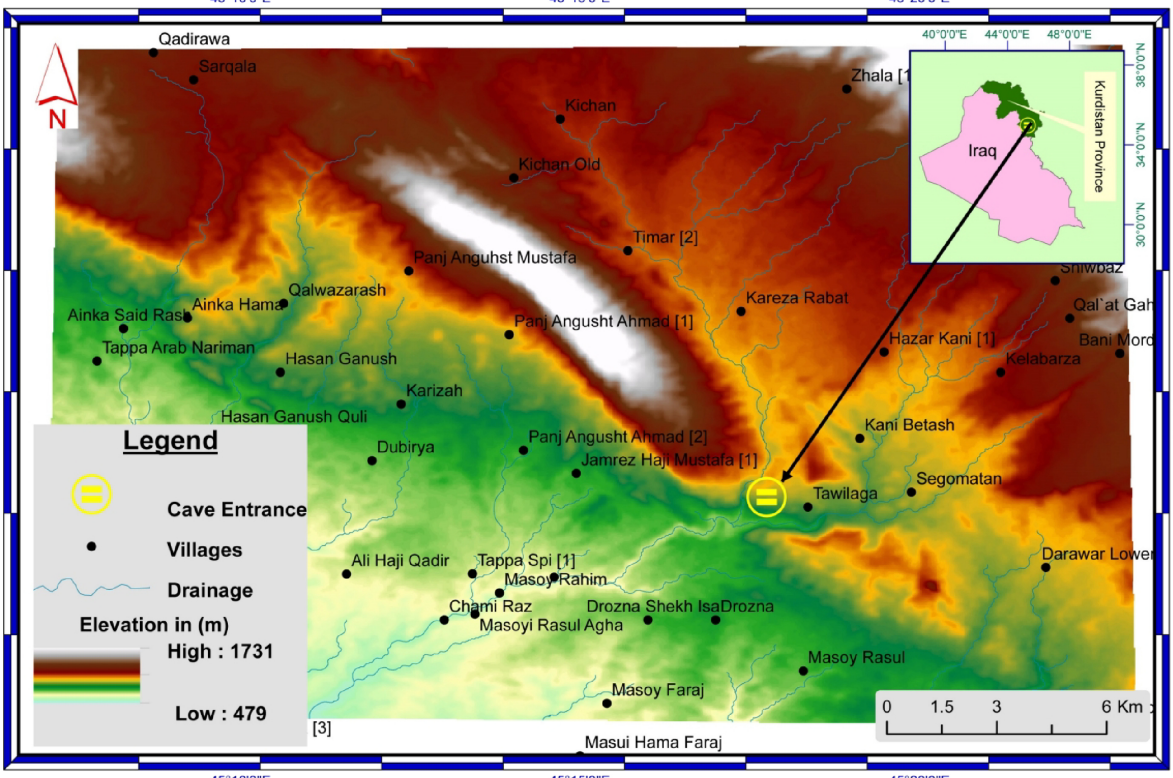
45°10'0"E
45°15'0"E
45°20'0"E
35°15'0"N
35°10'0"N
N
Qadirawa
Sarqala
Zhala [1]
Kichan
Kichan Old
Timar [2]
Panj Anguhst Mustafa
Qalwazarash
Ainka Hama
Ainka Said Rash
Tappa Arab Nariman
Hasan Ganush
Karizah
Hasan Ganush Quli
Dubirya
Panj Angusht Ahmad [1]
Panj Angusht Ahmad [2]
Jamrez Haji Mustafa [1]
Kareza Rabat
Hazar Kani [1]
Kelabarza
Kani Betash
Segomatan
Tawilaga
Darawar Lower
Ali Haji Qadir
Tappa Spi [1]
Masoy Rahim
Chami Raz
Masoyi Rasul Agha
Drozna Shekh Isa
Drozna
Masoy Rasul
Masoy Faraj
Masui Hama Faraj
[3]
Legend
Cave Entrance
Villages
Drainage
Elevation in (m)
High : 1731
Low : 479
0 1.5 3 6 Km
40°0'0"E
44°0'0"E
48°0'0"E
38°0'0"N
34°0'0"N
30°0'0"N
Iraq
Kurdistan Province

Figure 1

Entrance of the large gallery with rimstone dams and flutes show the direction of the paleoflow.

Left side of the large gallery characterized by the presence of flowstones, draperies and stalagmites.

Site 1 of small gallery characterized by the presence of small and broken stalagmites and soda straws.

Site 2 of small gallery characterized by the presence of flowstone and hill of soil.

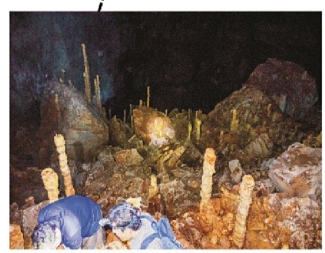

The right side of large gallery characterized by the presence of regular and long shaped stalagmites.

Figure 2

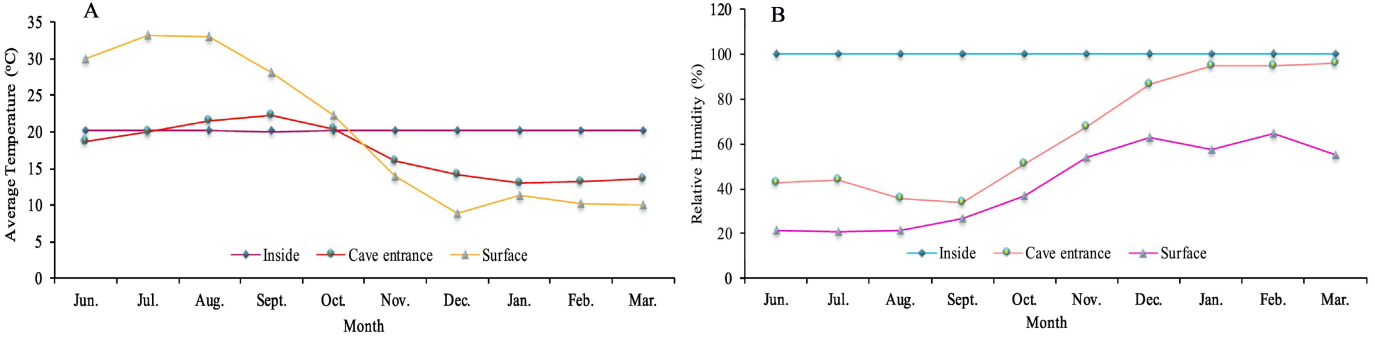
A
Average Temperature (°C)
35
30
25
20
15
10
5
0
Inside
Cave entrance
Surface
Jun.
Jul.
Aug.
Sept.
Oct.
Nov.
Dec.
Jan.
Feb.
Mar.
Month
B
Relative Humidity (%)
120
100
80
60
40
20
0
Inside
Cave entrance
Surface
Jun.
Jul.
Aug.
Sept.
Oct.
Nov.
Dec.
Jan.
Feb.
Mar.
Month

Figure 3

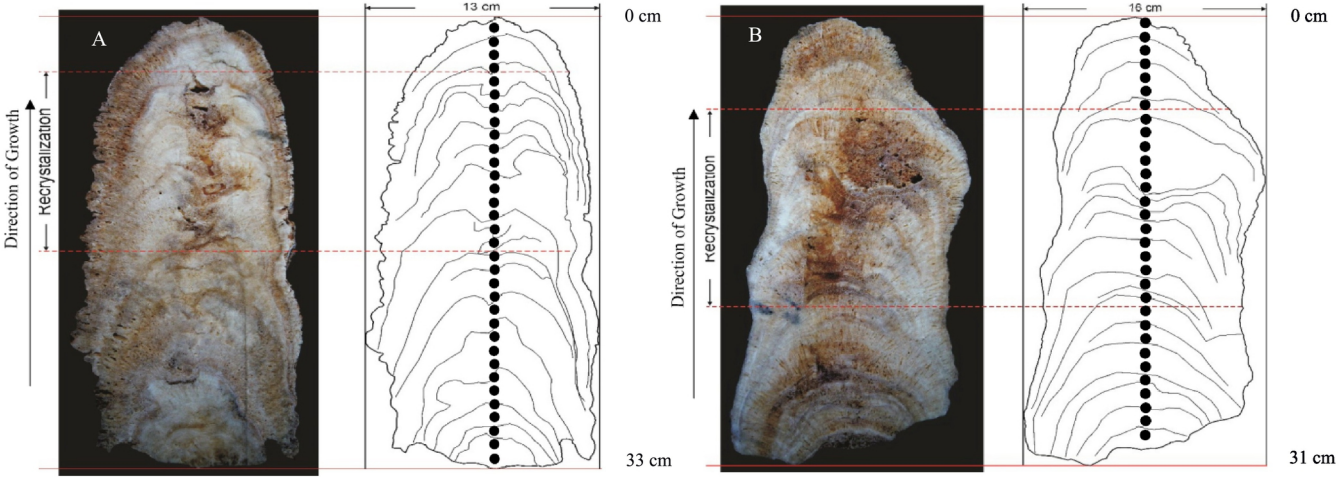
A
13 cm
0 cm
33 cm
Direction of Growth
Recrystalization
B
16 cm
0 cm
31 cm
Direction of Growth
Recrystalization

Figure 4

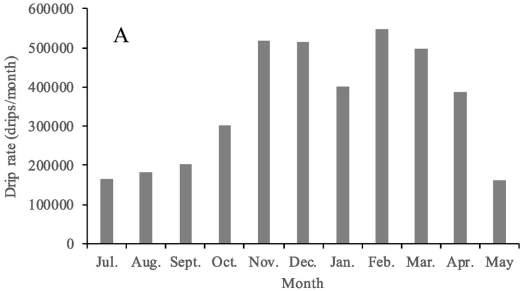
A
Drip rate (drips/month)
600000
500000
400000
300000
200000
100000
0
Jul.
Aug.
Sept.
Oct.
Nov.
Dec.
Jan.
Feb.
Mar.
Apr.
May
Month

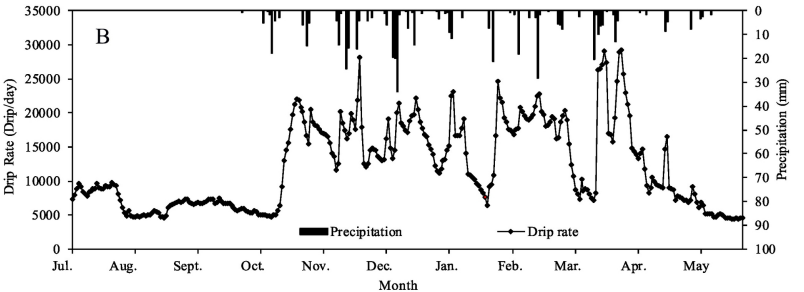
B
Drip Rate (Drip/day)
35000
30000
25000
20000
15000
10000
5000
0
Precipitation (mm)
0
10
20
30
40
50
60
70
80
90
100
Precipitation
Drip rate
Jul.
Aug.
Sept.
Oct.
Nov.
Dec.
Jan.
Feb.
Mar.
Apr.
May
Month

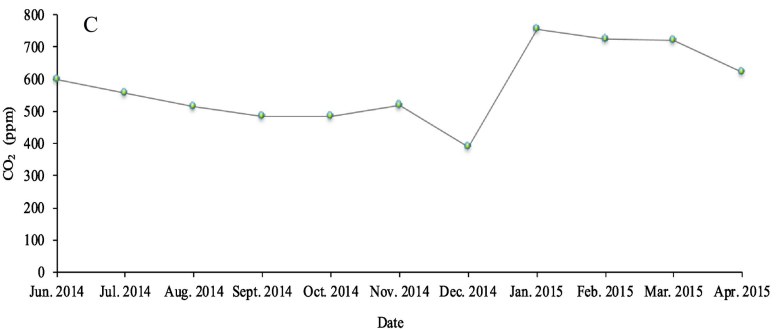
C
CO2 (ppm)
800
700
600
500
400
300
200
100
0
Jun. 2014
Jul. 2014
Aug. 2014
Sept. 2014
Oct. 2014
Nov. 2014
Dec. 2014
Jan. 2015
Feb. 2015
Mar. 2015
Apr. 2015
Date

Figure 5

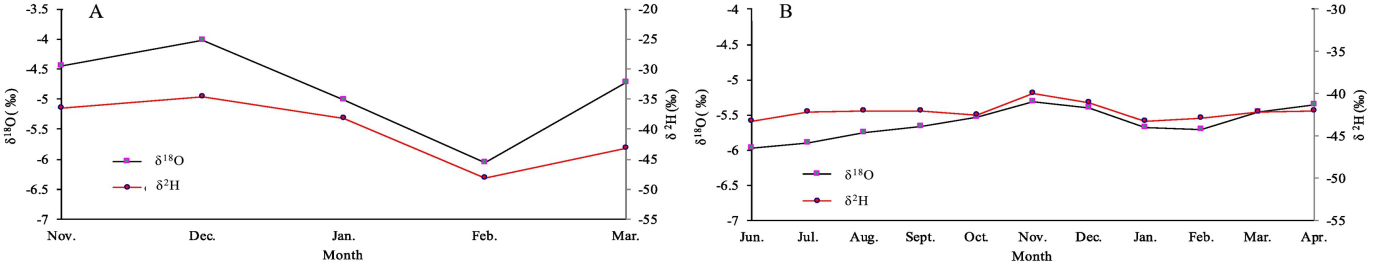
A
B
δ18O(‰)
δ2H(‰)
δ18O
δ2H
Month
Nov.
Dec.
Jan.
Feb.
Mar.
Jun.
Jul.
Aug.
Sept.
Oct.
Nov.
Dec.
Jan.
Feb.
Mar.
Apr.

Figure 6

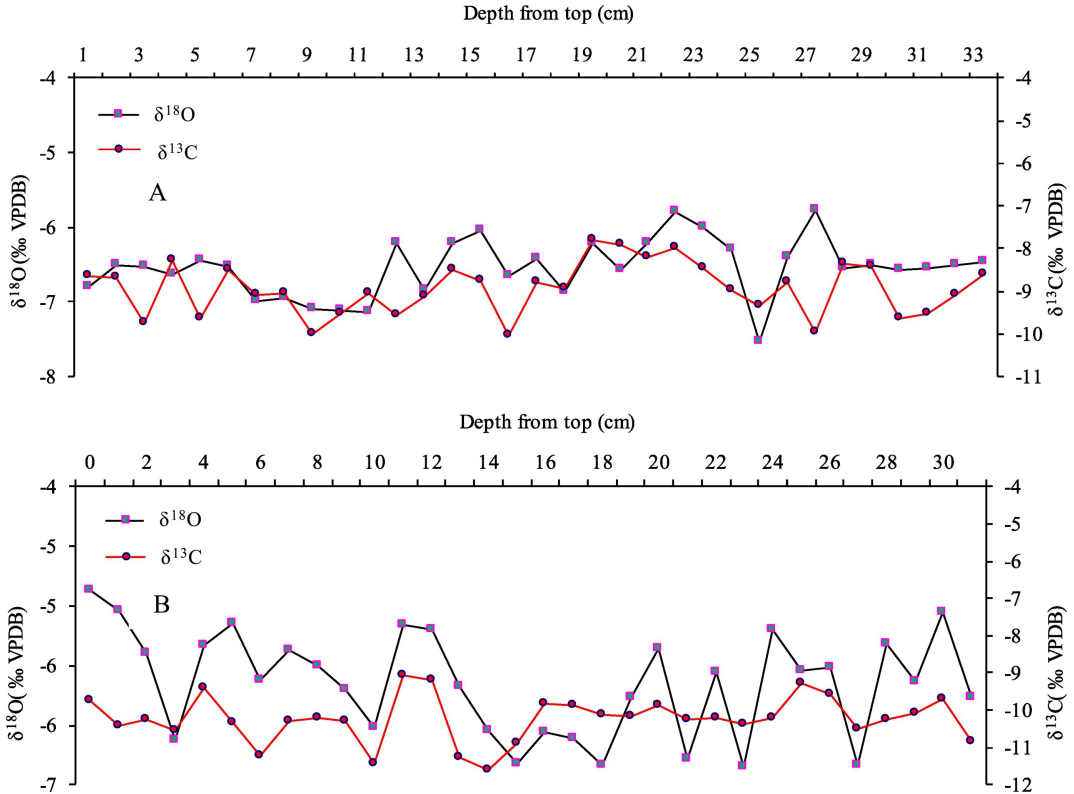
Depth from top (cm)
1 3 5 7 9 11 13 15 17 19 21 23 25 27 29 31 33
δ18O
δ13C
A
δ18O(‰ VPDB)
δ13C(‰ VPDB)
-4 -5 -6 -7 -8
-4 -5 -6 -7 -8 -9 -10 -11
Depth from top (cm)
0 2 4 6 8 10 12 14 16 18 20 22 24 26 28 30
δ18O
δ13C
B
δ18O(‰ VPDB)
δ13C(‰ VPDB)
-4 -5 -6 -7
-4 -5 -6 -7 -8 -9 -10 -11 -12

Figure 7

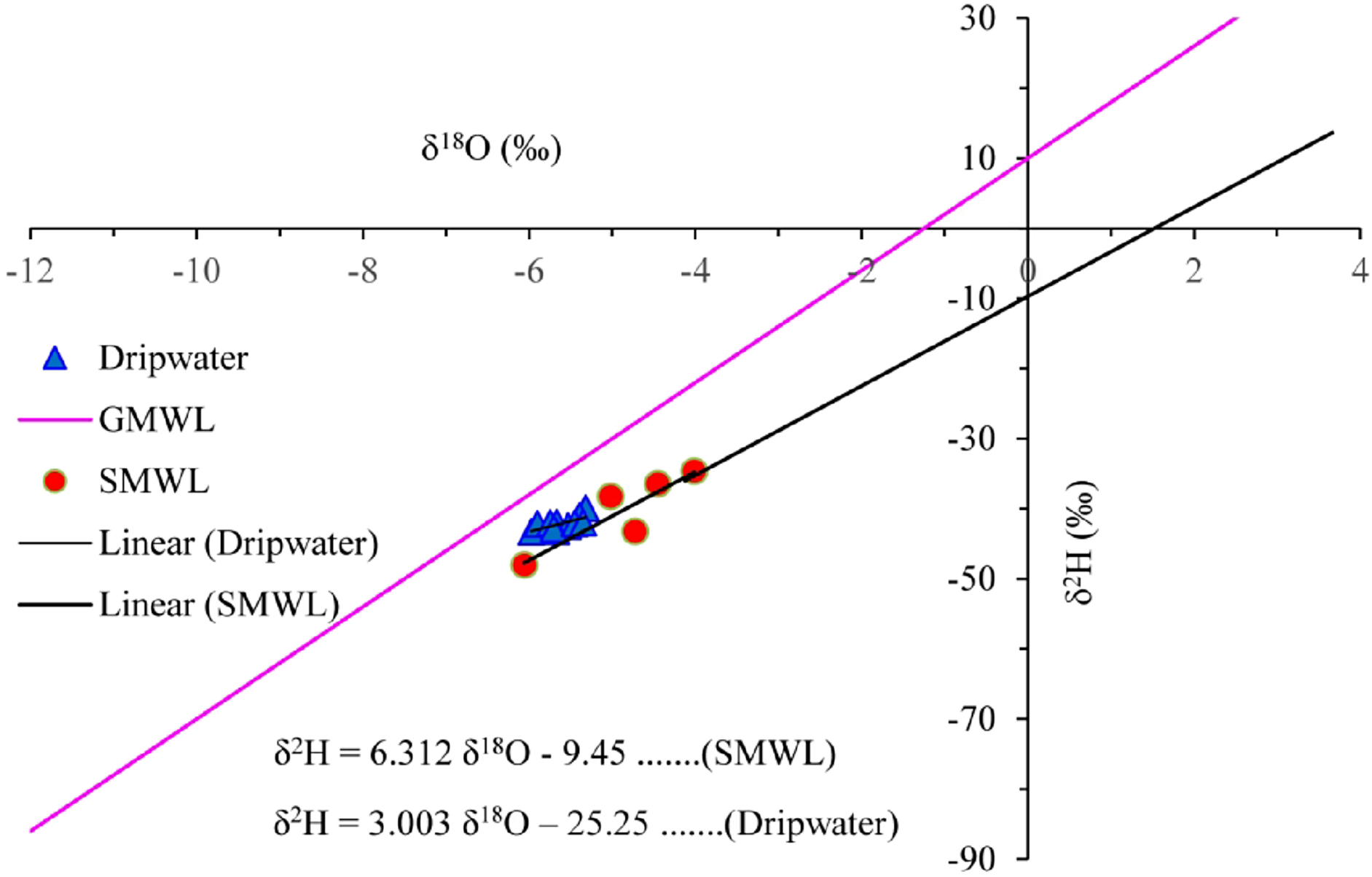
δ18O (‰)
30
10
-10
-30
-50
-70
-90
-12
-10
-8
-6
-4
-2
0
2
4
δ2H (‰)
Dripwater
GMWL
SMWL
Linear (Dripwater)
Linear (SMWL)
δ2H = 6.312 δ18O - 9.45 .....(SMWL)
δ2H = 3.003 δ18O – 25.25 .....(Dripwater)

Figure 8

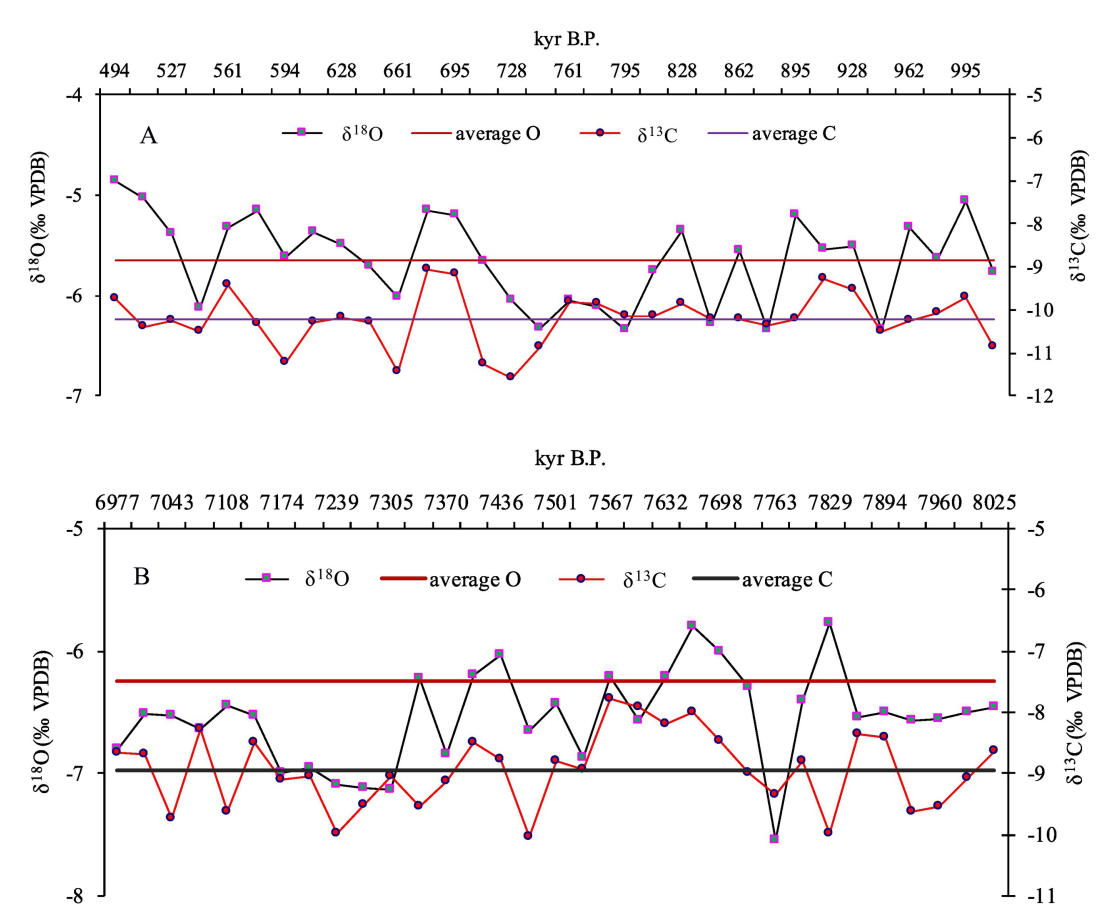
kyr B.P.
494 527 561 594 628 661 695 728 761 795 828 862 895 928 962 995
A
δ18O
average O
δ13C
average C
δ18O(‰ VPDB)
δ13C(‰ VPDB)
-4 -5 -6 -7
-5 -6 -7 -8 -9 -10 -11 -12
kyr B.P.
6977 7043 7108 7174 7239 7305 7370 7436 7501 7567 7632 7698 7763 7829 7894 7960 8025
B
δ18O
average O
δ13C
average C
δ18O(‰ VPDB)
δ13C(‰ VPDB)
-5 -6 -7 -8
-5 -6 -7 -8 -9 -10 -11

Figure 9